# Dynamic stabilization of cubic $CaSiO_3$ perovskite at high temperatures and pressures from *ab initio* molecular dynamics

Tao Sun,[1,*] Dong-Bo Zhang,[1] and Renata M. Wentzcovitch[1,2,†]

[1]*Department of Chemical Engineering and Materials Science, University of Minnesota, Minneapolis, Minnesota 55455, USA*

[2]*Minnesota Supercomputing Institute, University of Minnesota, Minneapolis, Minnesota 55455, USA*

(Received 10 July 2013; revised manuscript received 25 February 2014; published 26 March 2014)

The stability of cubic $CaSiO_3$ perovskite (CaPv) at high temperatures and pressures is investigated by vibrational normal-mode analysis. We compute power spectra of mode autocorrelation functions using a recently developed hybrid approach combining *ab initio* molecular dynamics with lattice dynamics. These power spectra, together with the probability distributions of atomic displacements, indicate that cubic CaPv is stabilized at $T \sim 600$ K and $P \sim 26$ GPa. We then utilize the concept of phonon quasiparticles to characterize the vibrational properties of cubic CaPv at high temperature and obtain anharmonic phonon dispersions through the whole Brillouin zone. Such temperature-dependent phonon dispersions pave the way for more accurate calculations of free-energy, thermodynamic, and thermoelastic properties of cubic CaPv at Earth's lower mantle conditions.

DOI: 10.1103/PhysRevB.89.094109 PACS number(s): 63.20.kg, 63.20.dk, 91.60.Hg

## I. INTRODUCTION

$CaSiO_3$ perovskite (CaPv) is believed to be the third most abundant mineral in the Earth's lower mantle (6 to 12 wt %). It is also the last major mantle phase whose structural and elastic properties have not been well characterized [1–4]. The structure of CaPv was initially proposed to be cubic with a space group $Pm\bar{3}m$ [5–8]. However, harmonic phonon calculations revealed that cubic CaPv contains unstable normal modes with imaginary frequencies at all pressures ($P$) [1]. Subsequent experiments also indicated that cubic CaPv is unstable at room temperature ($T$) [2,9,10], leading to the present understanding on the structure of CaPv, i.e., a slightly distorted noncubic structure, either tetragonal [1,11–13] or orthorhombic [14,15] at low $T$, which transforms into the cubic phase at high $T$. Unfortunately, the $P$-$T$ conditions under which cubic CaPv is stabilized are under debate, still. X-ray-diffraction experiments conducted by Komabayashi *et al*. [16] identified the transition temperature as between 490 and 580 K at 27 to 72 GPa, in accordance with earlier studies by Ono *et al*. [10] and Kurashina *et al*. [9], while a more recent experiment suggested CaPv remains noncubic with a space group $Pbnm$ or $Cmcm$ up to 18 GPa and 1600 K [17]. Resolving the stability of cubic CaPv at Earth's lower mantle conditions ($23 < P < 135$ GPa and $2000 < T < 4000$ K) is important for the interpretation of seismic data, as cubic and noncubic CaPv may have very different sound velocities [11,18].

The high-temperature stabilization of cubic CaPv has been the subject of several theoretical studies. Adams and Oganov conducted *ab initio* molecular dynamics (AIMD) in a metrically cubic supercell [15]. By examining the hydrostaticity of the time-averaged stress tensor, they found the transition temperature to cubic CaPv to be between 1000 and 2000 K. A similar conclusion was obtained by Stixrude *et al*. [11] using Landau mean-field theory. In contrast, AIMD carried out by Li *et al*. [19,20] found the hydrostatically compressed structure to be tetragonal up to 4000 K. The lack of consensus between theoretical and experimental studies calls for further investigations with new perspectives and methods.

Here we address the stability of cubic CaPv by computing its temperature-dependent phonon dispersion, which has not been determined yet. The underlying idea is that the frequency shifts of soft modes induced by temperature can be good indicators of displacive phase transitions [21,22]; i.e., once cubic CaPv is stabilized, all of its vibrational normal modes should be stable, having positive frequencies. The characterization of normal modes and the calculation of temperature-dependent phonon dispersions of CaPv are conducted using a recently developed computational scheme [23]. This scheme consists of two steps. In the first step, mode projected velocity autocorrelation functions and the corresponding power spectra, which numerically define phonon quasiparticles, are computed by projecting ionic velocities obtained from AIMD trajectories onto vibrational normal modes. After the existence of phonon quasiparticles is verified, renormalized phonon frequencies and lifetimes are extracted [23]. In the second step, effective dynamical matrices are constructed using the renormalized phonon frequencies and the phonon polarization vectors. Complete phonon dispersions and vibrational density of states are then obtained by Fourier interpolation. These dispersions can be used to determine accurately the entropy and free energy of cubic CaPv in the framework of the phonon gas model (PGM) [24–26].

The paper is organized as follows: we first review the method used in Sec. II. Simulation details are reported in Sec. III. Section IV contains our main results: dynamic stabilization of cubic CaPv and the corresponding temperature-dependent phonon dispersion. In Sec. V, we discuss how the system's vibrational entropy is affected by the temperature dependence of phonon frequencies. We also check the accuracy of our approach by comparing the calculated entropy with that predicted by the formally exact thermodynamic integration (TI) method. Conclusions are reported in Sec. VI.

*Present address: Key Laboratory of Computational Geodynamics, University of Chinese Academy of Sciences, Beijing 100049, China.

†wentz002@umn.edu.

 

## II. METHOD

As a method based on the PGM, the present approach [23] relies on the existence of phonon quasiparticles with well-defined frequencies and lifetimes [26]. While for simple materials this prerequisite can be verified by inelastic neutron or x-ray-scattering spectroscopy [27,28], at present such verification is not feasible for complex minerals such as CaPv. The present approach allows substantiating the existence of phonon quasiparticles from the start.

Consider an AIMD simulation conducted in a $N_1 \times N_2 \times N_3$ supercell; the power spectrum of the velocity autocorrelation function is defined as

$$\langle \mathbf{v}_{ls} \cdot \mathbf{v}_{ls} \rangle_\omega = \sum_\alpha \int_0^\infty \langle v_{ls\alpha}(0) v_{ls\alpha}(t) \rangle e^{i\omega t} dt, \tag{1}$$

where $\mathbf{v}_{ls}$ denotes the mass-weighted velocity of particle $s$ in the unit cell $l$. $v_{ls\alpha}$ is its $\alpha$-Cartesian component. In general $\langle \mathbf{v}_{ls} \cdot \mathbf{v}_{ls} \rangle_\omega$ contains multiple peaks. Each peak corresponds to a vibrational normal mode involving the particle labeled by $l$ and $s$. The total vibrational density of states (VDOS) of the supercell is given by $\sum_{ls} \langle \mathbf{v}_{ls} \cdot \mathbf{v}_{ls} \rangle_\omega$ [21,29].

To better resolve individual phonons, $\mathbf{v}_{ls}$ is first projected onto different wave vectors. Translational symmetry gives

$$\mathbf{v}_{\mathbf{q}s} = \sum_l \mathbf{v}_{ls} e^{-i\mathbf{q}\cdot\mathbf{R}_l}, \tag{2}$$

where the wave vector $\mathbf{q}$ is commensurate with the supercell size. The resulting power spectrum is

$$\langle \mathbf{v}^*_{\mathbf{q}s} \cdot \mathbf{v}_{\mathbf{q}s} \rangle_\omega = \sum_\alpha \int_0^\infty \langle v^*_{\mathbf{q}s\alpha}(0) v_{\mathbf{q}s\alpha}(t) \rangle e^{i\omega t} dt. \tag{3}$$

The spectrum $\sum_s \langle \mathbf{v}^*_{\mathbf{q}s} \cdot \mathbf{v}_{\mathbf{q}s} \rangle_\omega$ contains contributions from all the vibrational modes with wave vector $\mathbf{q}$ [29,30].

Complex materials such as CaPv contain several vibrational modes with very similar frequencies and their spectral profiles overlap in $\sum_s \langle \mathbf{v}^*_{\mathbf{q}s} \cdot \mathbf{v}_{\mathbf{q}s} \rangle_\omega$ . In these cases a further projection is necessary:

$$v_{\mathbf{q}j} = \sum_{s\alpha} v_{\mathbf{q}s\alpha} \hat{e}^*_\alpha(s|\mathbf{q}j), \tag{4}$$

where $\hat{\mathbf{e}}(s|\mathbf{q}j)$ is the polarization vector of the harmonic phonon with wave vector $\mathbf{q}$ and branch $j$. The power spectrum of the autocorrelation function for $v_{\mathbf{q}j}$ is simply

$$\langle v^*_{\mathbf{q}j} v_{\mathbf{q}j} \rangle_\omega = \int_0^\infty \langle v^*_{\mathbf{q}j}(0) v_{\mathbf{q}j}(t) \rangle e^{i\omega t} dt. \tag{5}$$

A single peak with a Lorentzian line shape in $\langle v^*_{\mathbf{q}j} v_{\mathbf{q}j} \rangle_\omega$ indicates a well-defined phonon quasiparticle [26]. The peak position corresponds to the renormalized phonon frequency $\tilde{\omega}_{\mathbf{q}j}$. The linewidth is inversely proportional to the phonon lifetime [26]. Inspection of the $\langle v^*_{\mathbf{q}j} v_{\mathbf{q}j} \rangle_\omega$ spectra can verify whether phonon quasiparticles are well defined in the system [26]. If $\langle v^*_{\mathbf{q}j} v_{\mathbf{q}j} \rangle_\omega$ resembles Lorentzian functions, then their renormalized frequencies $\tilde{\omega}_{\mathbf{q}j}$ can be thus obtained. This way, $\tilde{\omega}_{\mathbf{q}j}$ of all phonons sampled by the supercell can be obtained.

The next step is to calculate renormalized phonon dispersions in the whole Brillouin zone. Recall that for harmonic phonons $\sum_{s'\beta} D_{\alpha\beta}(ss'|\mathbf{q}) \hat{e}_\beta(s'|\mathbf{q}j) = \omega^2_{\mathbf{q}j} \hat{e}_\alpha(s|\mathbf{q}j)$, where $\mathbf{D}$ is the harmonic dynamical matrix. Replacing $\omega^2_{\mathbf{q}j}$ with $\tilde{\omega}^2_{\mathbf{q}j}$ and applying the orthonormality condition of polarization vectors one gets an effective dynamical matrix $\tilde{\mathbf{D}}$ as

$$\tilde{D}_{\alpha\beta}(ss'|\mathbf{q}) = \sum_j \tilde{\omega}^2_{\mathbf{q}j} \hat{e}_\alpha(s|\mathbf{q}j) \hat{e}^*_\beta(s'|\mathbf{q}j). \tag{6}$$

The effective dynamical matrix $\tilde{\mathbf{D}}$ has the same eigenvectors as its harmonic counterpart $\mathbf{D}$, while its eigenvalues are renormalized from $\omega^2_{\mathbf{q}j}$ to $\tilde{\omega}^2_{\mathbf{q}j}$. A discrete Fourier transformation on $\tilde{\mathbf{D}}$ gives an effective harmonic force constant matrix in real space. The dynamical matrix of arbitrary wave vector $\mathbf{q}$ can then be built and diagonalized to get renormalized phonon frequencies. Note that, in constructing the real space force constant matrix for polar crystals such as CaPv, short-ranged forces need to be separated from long-ranged dipole-dipole interactions to ensure rapid spacial convergence of the interatomic force constants [31].

The projection as defined in Eq. (4) assumes tacitly that the polarization vectors of phonon quasiparticles at finite temperatures are the same as those of harmonic phonons $\hat{\mathbf{e}}(s|\mathbf{q}j)$, and anharmonic effects are taken into account by the renormalized phonon frequencies and lifetimes only. This assumption is in accordance with standard many-body theory, where $\hat{\mathbf{e}}(s|\mathbf{q}j)$ can be chosen as an unperturbed basis and each phonon acquires through anharmonic interactions a temperature-dependent self-energy [32]. The real and imaginary parts of the phonon self-energy correspond to the frequency shift and the inverse lifetime, respectively [26,32]. It will be shown that this assumption works well in the temperature range where cubic CaPv is stable.

## III. SIMULATION DETAILS

Simulations were conducted using the plane-wave pseudopotential method as implemented in the QUANTUM ESPRESSO software [33]. Harmonic phonon frequencies and polarization vectors were calculated using density-functional perturbation theory (DFPT) [34]. The local-density approximation (LDA) [35] was chosen for the exchange-correlation functional as previous calculations showed LDA gives the best equation of states for CaPv [11–13]. The pseudopotentials for Ca, Si, and O were generated by Vanderbilt's method [36]. The reference electronic configurations and the core radii for all angular quantum numbers $l$ (in parentheses) are $3s^2 3p^6 4s^1 4p^0 3d^0$ (2.0 a.u.), $3s^2 3p^1 3d^0$ (1.6 a.u.), and $2s^2 2p^4$ (1.4 a.u.) for Ca, Si, and O, respectively. The static equation of state and harmonic phonon dispersions of cubic CaPv determined using these pseudopotentials are in excellent agreement with those in literature [1,12].

CaPv was simulated with a $2 \times 2 \times 2$ cubic supercell containing 40 atoms. The $2 \times 2 \times 2$ supercell is the minimum size to sample the unstable phonon modes at $\mathbf{q}$ vectors $\mathbf{R}$ $(\frac{1}{2}, \frac{1}{2}, \frac{1}{2})$ and $\mathbf{M}$ $(\frac{1}{2}, \frac{1}{2}, 0)$. On the other hand, our calculations confirmed that this cell is sufficiently large to get spatially converged interatomic force constants for harmonic phonon interpolations [1,12]. Because the anharmonic parts of interatomic forces have shorter ranges than the harmonic components [37], the $2 \times 2 \times 2$ cell with 40 atoms should

also be adequate to obtain converged effective harmonic force constants. The plane-wave energy cutoff was set to 36 Ry. A higher cutoff (60 Ry) changed the equilibrium lattice parameter of cubic CaPv by merely 0.001 Å. Since previous studies have shown insufficient **k**-point sampling can bias the calculated stresses and lead to incorrect hydrostatic structures [11], we carefully checked the convergence of stresses with respect to **k**-point sampling. We found that using the gamma point only would cause errors of more than 1 GPa in the calculated stresses, while the stresses calculated on a shifted $2 \times 2 \times 2$ Monkhorst-Pack **k**-point mesh [38] differed from those on a shifted $4 \times 4 \times 4$ **k**-point mesh by less than 0.02 GPa. Thus we chose the shifted $2 \times 2 \times 2$ **k**-point mesh (four **k** points) for all our calculations.

To study the intrinsic temperature dependence of phonon frequencies, we conducted Born-Oppenheimer molecular dynamics [39] using the $NVT$ ensemble with a Nose-Hoover thermostat [40]. The temperature ranged from 10 to 4500 K. The lattice parameter of the unit cell was set to 3.45 Å. It corresponds to a static pressure of 23 GPa: the pressure at the top of the lower mantle. At 600 K, this volume corresponds to a pressure of 26 GPa. The time step was set to 0.97 fs, about 1/30 of the period of the highest-frequency phonon in the system. To minimize statistical error fairly long simulations (>50 ps) were carried out at each temperature and the maximum entropy method [41] was used to compute the power spectra of velocity autocorrelation functions.

## IV. RESULTS

### A. Emergence of the cubic symmetry

Before studying vibrational properties, it is useful to first identify the system's equilibrium configuration. The ideal cubic structure [$a^0a^0a^0$ in Glazer's notation [42], as illustrated in Fig. 1(a)] contains modes with imaginary frequencies and is not the equilibrium structure at 0 K, even though it may become the preferred structure at high temperatures because it is more symmetric and has higher entropy. Energetically more stable structures can be obtained by relaxing the atoms associated with these unstable modes, tilts (or rotations) of the $SiO_6$ octahedra [11–13]. A representative tilted structure is shown in Fig. 1(b). In the following we determine the

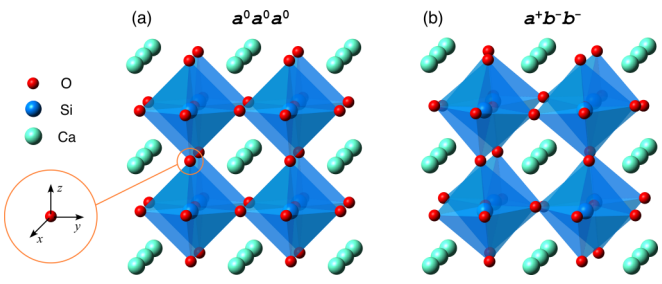


FIG. 1. (Color online) CaPv in a $2 \times 2 \times 2$ cubic supercell. (a) The ideal cubic structure ($a^0a^0a^0$) being dynamically unstable at 0 K. (b) The $a^+b^-b^-$ structure with the atomic degrees of freedom fully relaxed. It is 5.5 meV/atom more stable than $a^0a^0a^0$. Its tilting angles in the $x$, $y$, and $z$ directions are 1.4, 4.5, and 4.5°, respectively. Harmonic phonon calculations indicate that all of its vibrational frequencies are positive.

equilibrium structure at relevant temperatures by inspecting the probability distributions of atomic displacements.

Figure 2(a) shows the probability distributions of atomic displacements with respect to the perfect cubic structure at 1000 K. For all types of atoms, we see bell-shaped distribution curves centered at zero displacements. Since the probability distribution of atomic displacements is maximal at the equilibrium position around which the atom oscillates [43], we conclude that the equilibrium structure of CaPv at 1000 K is $a^0a^0a^0$. Note that the distribution function of O displacements is not identical in the three Cartesian directions. It is narrower (smaller variance) in the $z$ direction compared to the $x$ or $y$ direction. The variance of the distribution is the mean-square displacement and the origin of this anisotropy can be understood as follows: O displacements in the $z$ direction are associated with $SiO_6$ octahedral stretching. O displacements in the $x$ or $y$ direction are related to $SiO_6$ octahedral tilting (rotating). The mean-square displacement in a certain direction equals $k_BT/M\omega_0^2$, where $\omega_0$ is the frequency of the vibrational mode polarized in that direction [21]. Because tilting modes in general are lower in frequency than stretching modes, the mean-square displacement in the $z$ direction is smaller than in the $x$ or $y$ direction.

At lower temperature, the atomic vibrations become more complex. Although the distributions of Ca, Si, and O in the $z$-direction displacements still peak at zero, a splitting of the distribution peak of O in $x$ and $y$ directions develops below 600 K. The split peaks at 150 K locate at 0.12 Å, as shown in Fig. 2(b). Because the distribution function has two maxima located at nonzero displacements, the equilibrium structure at low T is no longer $a^0a^0a^0$ and is not unique. Since the splitting is observed only for the O displacements in the $x$ and $y$ directions, the corresponding equilibrium structures contain tilted $SiO_6$ octahedra. In this regard, O displacements of ±0.12 Å correspond to tilting angles of ±4.0°. In the MD simulated evolution, atoms first oscillate with respect to one of the equilibrium structures with a tilting angle of $+\theta$. As $SiO_6$ octahedra switch their tilting directions due to thermal fluctuations, atoms will oscillate around a different tilted structure with opposite tilting angle ($-\theta$). Such hopping among different tilted structures gives rise to two peaks that are nearly symmetric in the distribution function. At $T > 600$ K, entropic effects become stronger and the energetic preference of tilted structures becomes less important, and the two peaks in the distribution function start to merge into a single one centered at zero displacement, indicating that the undistorted cubic structure is the equilibrium configuration.

In our simulation, the time-averaged stress tensors are hydrostatic, i.e., $\langle\sigma_{xx}\rangle = \langle\sigma_{yy}\rangle = \langle\sigma_{zz}\rangle$, $\langle\sigma_{xy}\rangle = \langle\sigma_{xz}\rangle = \langle\sigma_{yz}\rangle = 0$, even at low $T$ (e.g., 50 K). This is in contrast with previous calculations by Adams and Oganov [15] and Li *et al.* [19,20]. In these calculations the **k**-point sampling is limited to the Gamma point only, which is insufficient to get fully converged stresses. The apparent hydrostaticity of the time-averaged stress tensor is due to the fact that $SiO_6$ octahedrons switch their tilting directions during the MD evolution [15,20] and the instantaneous nonhydrostatic deviations get canceled in the time average. Still, there is a fundamental difference, as shown in Fig. 3. At low $T$, the correlation function of the off-diagonal component of the stress tensor $\langle\sigma_{yz}(0)\sigma_{yz}(t)\rangle/\langle\sigma_{yz}\rangle^2$ decays

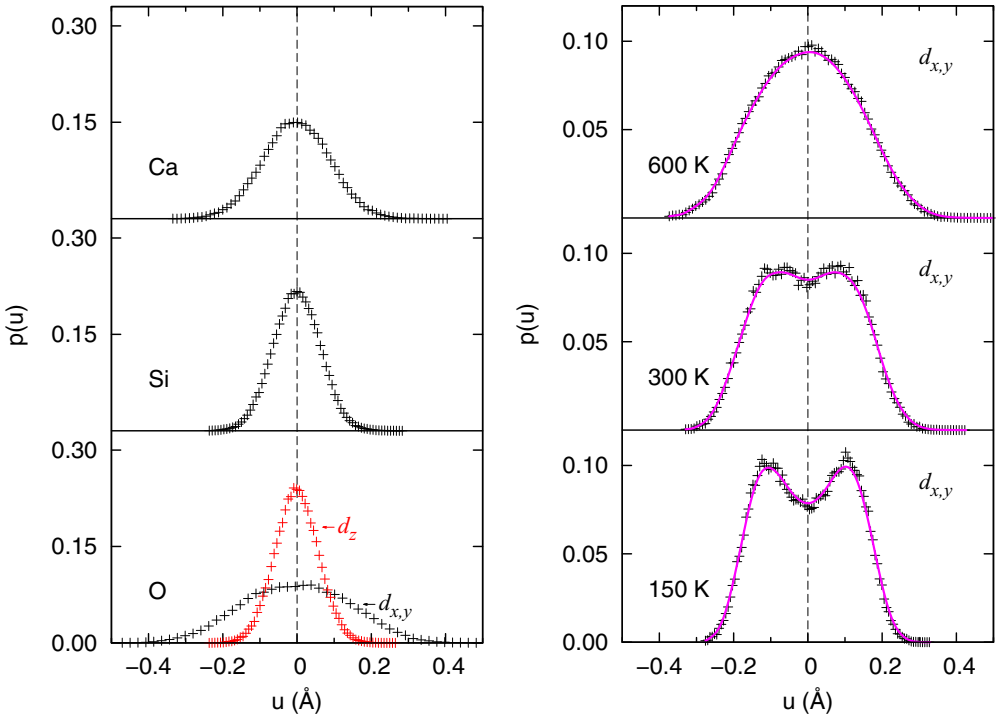


FIG. 2. (Color online) (a) Probability distributions of atomic displacements with respect to the ideal cubic structure ($a^0a^0a^0$ in Glazer's notation [42]) at $T = 1000$ K. For Ca and Si atoms, the distributions of atomic displacements in the three Cartesian directions are the same, while for O atoms displacements in the $z$ direction (octahedral stretching) are more restricted than displacements in the $x$ or $y$ direction (octahedral tilting). (b) Distributions of the O displacements in the $x$ or $y$ direction (octahedral tilting) with respect to the ideal cubic structure ($a^0a^0a^0$) at various temperatures.

slowly, indicating that the system is nonhydrostatic in the time scale of hundreds of femtoseconds. It decays much faster at high $T$, and the system is effectively hydrostatic once the decay time is comparable to or less than the average vibrational period (∼60 fs). In this high $T$ hydrostatic regime (⩾600 K), pressure is defined as $(\langle\sigma_{xx}\rangle + \langle\sigma_{yy}\rangle + \langle\sigma_{zz}\rangle)/3$. Its temperature dependence is given by

$$P = P_0 + \gamma \frac{(3N-3)k_B T}{V},$$

where $P_0$ is the static pressure; $N$ and $V$ are the total number of atoms and the volume of the simulation cell, respectively; and $\gamma$ is the thermal Grüneisen parameter. In this case, $P_0$ equals

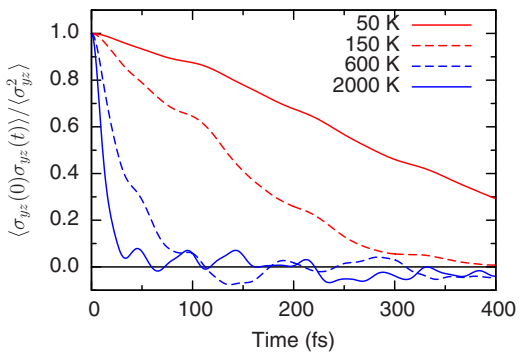


FIG. 3. (Color online) Correlation of an off-diagonal component of the stress tensor $\sigma_{yz}$ at various temperatures.

23 GPa, $N$ equals 40, and $V$ equals 327.23 Å$^3$. We find that $\gamma$ shows little temperature dependence and equals 1.34, in good agreement with that of Adams and Oganov (1.43) [15] and of Li *et al.* (1.37) [19,20].

The transition temperature (∼600 K) identified from the distribution of atomic displacements is close to some experimental observations, where the transition temperature was determined to be between 490 and 580 K [10,16,44]. While the agreement is good, we note our approach is rather phenomenological. In particular, the fixed cubic simulation cell excludes the fluctuations of lattice strains, which can be important. The more rigorous way to determine phase boundaries is to compare directly the free energies of competing phases. The renormalized phonon frequencies presented in the following sections make possible more accurate determination of the free energy of cubic CaPv.

### B. Phonons of cubic CaPv

The concept of the phonon is useful to characterize lattice vibrations. Here we employ the approach described above, which numerically defines phonon quasiparticles, to study the evolution of soft modes with temperature in cubic CaPv. This result has implications on the stabilization of the cubic CaPv phase.

We have carried out AIMD on a $2 \times 2 \times 2$ cubic supercell. Four inequivalent $\mathbf{q}$ vectors of the primitive cubic perovskite cell were sampled: $\mathbf{\Gamma}(0,0,0)$, $\mathbf{X}(0,0,\frac{1}{2})$, $\mathbf{M}(0,\frac{1}{2},\frac{1}{2})$,

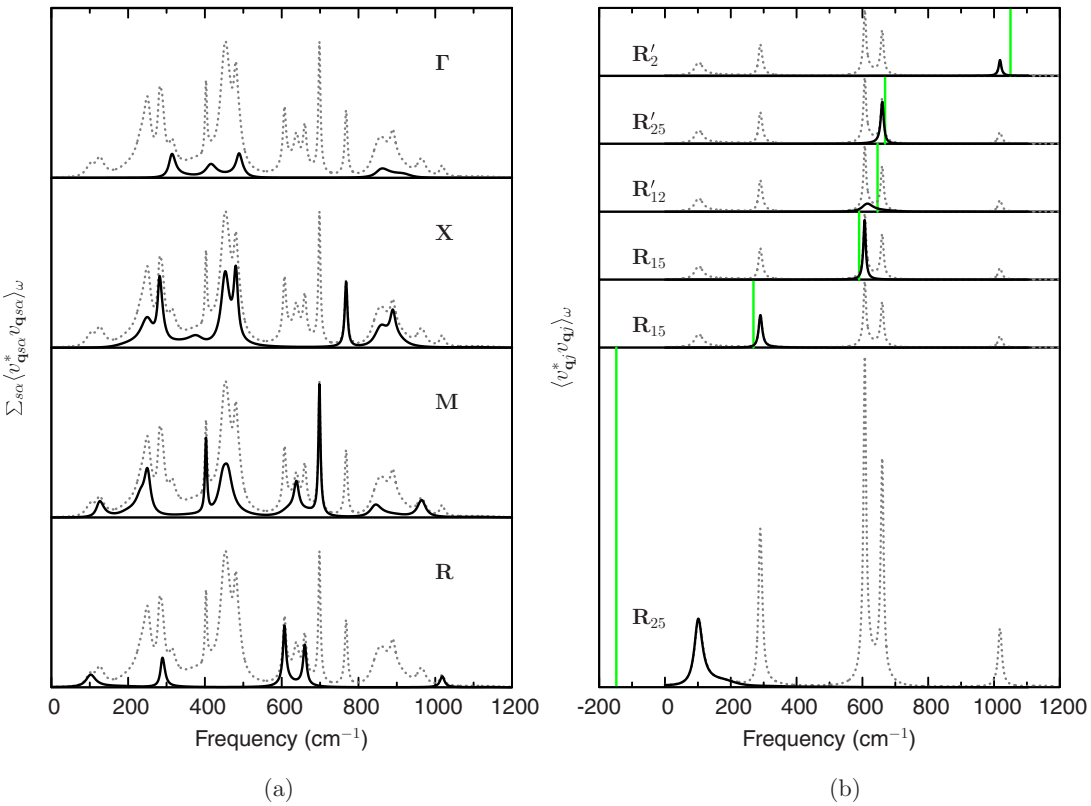


FIG. 4. (Color online) (a) Power spectrum of the velocity autocorrelation functions projected on different wave vectors. Dotted lines correspond to the total $\sum_{ls}\langle \mathbf{v}_{ls}\cdot\mathbf{v}_{ls}\rangle_\omega$. (b) Power spectrum of individual mode autocorrelation functions with $\mathbf{q}$ vector $\mathbf{R}$ $(\frac{1}{2},\frac{1}{2},\frac{1}{2})$ . Dotted lines correspond to the $\sum_s\langle \mathbf{v}^*_{\mathbf{q}s}\cdot\mathbf{v}_{\mathbf{q}s}\rangle_\omega$ at $\mathbf{R}$. The temperature is 1000 K.

and $\mathbf{R}(\frac{1}{2},\frac{1}{2},\frac{1}{2})$. Our approach enables calculations of the total power spectra $\sum_{ls}\langle \mathbf{v}_{ls}\cdot\mathbf{v}_{ls}\rangle_\omega$, the $\mathbf{q}$-projected power spectra $\sum_s\langle \mathbf{v}^*_{\mathbf{q}s}\cdot\mathbf{v}_{\mathbf{q}s}\rangle_\omega$, and the mode projected power spectra $\langle v^*_{\mathbf{q}j} v_{\mathbf{q}j}\rangle_\omega$. Results obtained at 1000 K are summarized in Fig. 4. Figure 4(a) shows $\sum_s\langle \mathbf{v}^*_{\mathbf{q}s}\cdot\mathbf{v}_{\mathbf{q}s}\rangle_\omega$ at the four MD sampled $\mathbf{q}$ vectors (solid lines). In the background, the total power spectra $\sum_{ls}\langle \mathbf{v}_{ls}\cdot\mathbf{v}_{ls}\rangle_\omega$ is also shown for comparison (dotted lines). $\sum_s\langle \mathbf{v}^*_{\mathbf{q}s}\cdot\mathbf{v}_{\mathbf{q}s}\rangle_\omega$ contains the contribution from all the modes at wave vector $\mathbf{q}$. For cubic CaPv, there are 15 such modes. Although several peaks can be identified from $\sum_s\langle \mathbf{v}^*_{\mathbf{q}s}\cdot\mathbf{v}_{\mathbf{q}s}\rangle_\omega$, corresponding to inequivalent vibrational modes, e.g, the case for $\mathbf{q}=\mathbf{\Gamma}$, the spectra of individual modes are not available. This is because there are modes whose frequencies are so close that their spectra overlap with each other, in contrast with the situation in simple crystals, e.g., MgO [45]. Fortunately, our approach allows the calculation of the power spectra for individual modes, $\langle v^*_{\mathbf{q}j} v_{\mathbf{q}j}\rangle_\omega$, i.e., the formalism encapsulated in Eqs. (4) and (5). Note that in Eq. (4) the polarization vector $\hat{\mathbf{e}}(s|\mathbf{q}j)$ is obtained with the perfect cubic structure $a^0a^0a^0$. Mode projected power spectra are shown in Fig. 4(b) for those modes at the wave vector $\mathbf{R}$. The convention of R. A. Cowley (see [46,47]) is used to indicate the symmetries of these modes. The spectrum of each mode with a single peak with a Lorentzian line shape indicates that the phonon quasiparticle is well defined. It is interesting to point out that the threefold degenerate $R_{25}$ modes having a harmonic frequency of $148i$ cm$^{-1}$ now have a real frequency of 102 cm$^{-1}$, as seen in Fig. 4(b). Similar effects are also found in other modes with imaginary harmonic frequencies, e.g., the $M_2$ mode with wave vector $\mathbf{M}$. This indicates that the cubic phase at 1000 K is dynamically stable.

At low $T$, where cubic CaPv is unstable, normal-mode projections using the polarization vectors of harmonic phonons can be futile. This is illustrated in Fig. 5, which shows the power spectra of the mode autocorrelation function of $R_{25}$ with $\mathbf{q}$ vector $\mathbf{R}$. At 150 K the spectrum contains two well-separated peaks and does not represent a well-defined phonon quasiparticle. The breakdown of normal-mode projections at low $T$ is not surprising; after all, we are using the polarization vectors of harmonic phonons of the perfect cubic structure $a^0a^0a^0$ to carry out the projection, while in this temperature regime the equilibrium structure around which the atoms oscillate is not $a^0a^0a^0$, as illustrated in Fig. 2. The extra peak in the power spectrum gets diminished at $T\sim 600$ K, consistent with the fact that the equilibrium structure takes on $a^0a^0a^0$ at this temperature.

The above analysis of normal-mode spectra indicates that it is proper to employ the concept of the phonon quasiparticle to depict lattice vibrations of cubic CaPv at $T>600$ K. Figure 6 shows the temperature dependence of phonon frequencies of cubic CaPv obtained under constant volume conditions, where the frequency shifts are caused by intrinsic temperature effects only (without thermal expansion). To compare the strength of intrinsic anharmonicity of each mode, frequencies are normalized by those at 600 K. We find that, for modes with

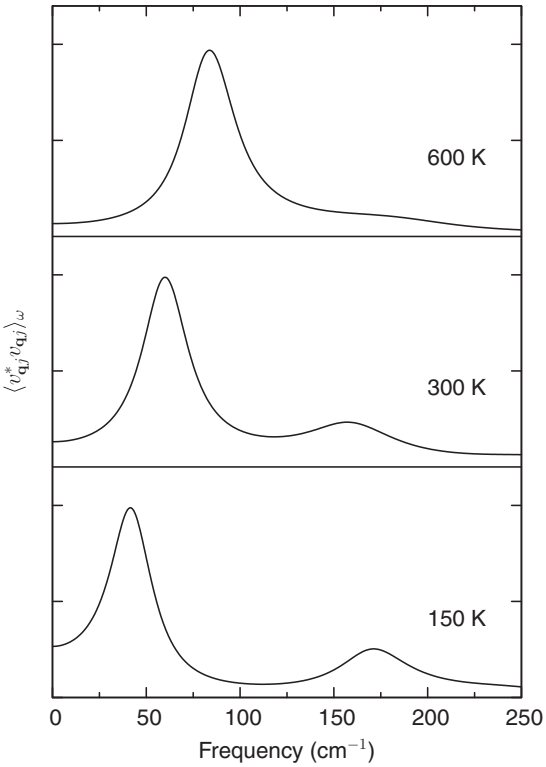


FIG. 5. Power spectra of the mode autocorrelation function of $R_{25}$ with $\mathbf{q}$ vector $\mathbf{R}$ $(\frac{1}{2}, \frac{1}{2}, \frac{1}{2})$ at low temperatures.

positive harmonic frequencies, temperature induced frequency shifts are relatively small, mostly within 5% up to 3500 K. Among these modes, some, e.g., $X'_5(451)$, show positive shifts that are nearly linear in $T$, and others, such as $X'_4(895)$, show negative shifts that are also linear in $T$. This linear $T$ dependence is consistent with lowest-order perturbation theory [24–26]. Frequency shifts can be either positive or negative, depending on the details of anharmonic interactions [37]. There are also modes whose frequencies are nearly temperature independent, such as $\Gamma_{15}(879)$ with wave vector $\mathbf{\Gamma}$. This suggests anharmonic effects are particularly weak for this mode, or alternatively a cancellation of contributions from the third- and fourth-order anharmonic force constants [26,37]. The largest relative frequency shifts are observed in modes that were unstable at 0 K. For instance, from 600 to 3500 K the frequency of $M_2(113)$ increases by 62.5%. The frequency of $R_{25}(85)$ nearly doubles. Clearly, the unstable normal modes at 0 K are also the most anharmonic ones. Their renormalized frequencies show a temperature dependence of $\sqrt{T}$, which seems to be consistent with the soft-mode model [21,22].

Having obtained the phonon frequencies of the $2 \times 2 \times 2$ supercell, we now consider phonon dispersions in the whole Brillouin zone. Following the procedure described in Sec. II, we obtain renormalized phonon dispersions as shown in Fig. 7. The LO-TO splitting effect, absent in supercell calculations, is taken into account by adding a nonanalytic contribution to the dynamical matrix in the long-wavelength limit [34]. We find that for stable branches (positive harmonic frequencies) the renormalized and harmonic phonon dispersions are not very different. This is consistent with results shown in Fig. 6: the temperature induced frequency shifts of such modes are relatively small. In contrast, the frequencies of unstable branches (imaginary harmonic frequencies) get lifted to positive frequencies in the renormalized phonon dispersions. At 1000 K, cubic CaPv is stable with respect to normal-mode displacements of any wavelength.

Recently Hellman *et al.* [28] proposed a new method to study lattice dynamics of anharmonic solids. The basic idea of the method is to find a set of effective harmonic force constants that give the best fit of the potential-energy surface generated by AIMD. This method has been successfully applied to simple metallic materials that were unstable at 0 K but get stabilized at high $T$. Here we use Hellman *et al.*'s method to cross-check our approach. As shown in Fig. 7, while in some parts the phonon frequencies obtained from Hellman *et al.*'s method are slightly smaller than those from the velocity autocorrelation functions, the overall agreement between the two methods is quite good. However, the present approach has the advantage that it gives more complete information on the dynamics of phonon quasiparticles. Besides renormalized phonon frequencies to compute thermodynamic properties, it also yields phonon lifetimes which can be used to determine lattice thermal conductivity [26,30].

## V. DISCUSSION

Here we discuss how the temperature dependence of phonon frequencies affects the system's vibrational entropy. We also check the accuracy of our approach by comparing the anharmonic entropy calculated from renormalized phonon frequencies with that given by the formally exact thermodynamic integration (TI) method [48]. This serves as a benchmark for future calculations of thermodynamic properties of cubic CaPv.

In the PGM, the vibrational entropy $S_{\text{vib}}$ is given by

$$S_{\text{vib}} = k_B \sum_{\mathbf{q}j} [(n_{\mathbf{q}j} + 1)\ln(n_{\mathbf{q}j} + 1) - n_{\mathbf{q}j} \ln n_{\mathbf{q}j}], \quad (7)$$

where $n_{\mathbf{q}j}$ is the Bose-Einstein distribution $[\exp(\hbar\Omega_{\mathbf{q}j}/k_B T) - 1]^{-1}$. In the semiclassical approximation, the frequencies of quasiparticles $\Omega_{\mathbf{q}j}$ are substituted by the renormalized frequencies $\tilde{\omega}_{\mathbf{q}j}$ extracted from MD [21]. This approximation works well especially at high $T$, where quantum effects are negligible.

In the current simulation, cubic CaPv is stable only at $T \geqslant$ 600 K. Thus, to measure anharmonic effects in cubic CaPv, we use renormalized frequencies at 600 K as a reference and define the anharmonic vibrational entropy $S_A$ as

$$S_A = S_{\text{vib}}\{\tilde{\omega}(T)\} - S_{\text{vib}}\{\tilde{\omega}(600\,\text{K})\}, \quad (8)$$

where $S_{\text{vib}}\{\tilde{\omega}(T)\}$ denotes vibrational entropy calculated from Eq. (7) using the renormalized phonon frequencies at the corresponding temperature and $S_{\text{vib}}\{\tilde{\omega}(600\,\text{K})\}$ corresponds to the vibrational entropy computed from Eq. (7) with phonon frequencies fixed at those of 600 K. For comparison we also calculate $S_A$ by the TI approach [26,48]. Since the ideal cubic structure $a^0a^0a^0$ contains unstable modes with imaginary frequencies, the relaxed structure $a^+b^-b^-$ shown in Fig. 1(b) was chosen as the reference harmonic system to carry out TI calculation. Similar to [23] and [26], we first evaluate the

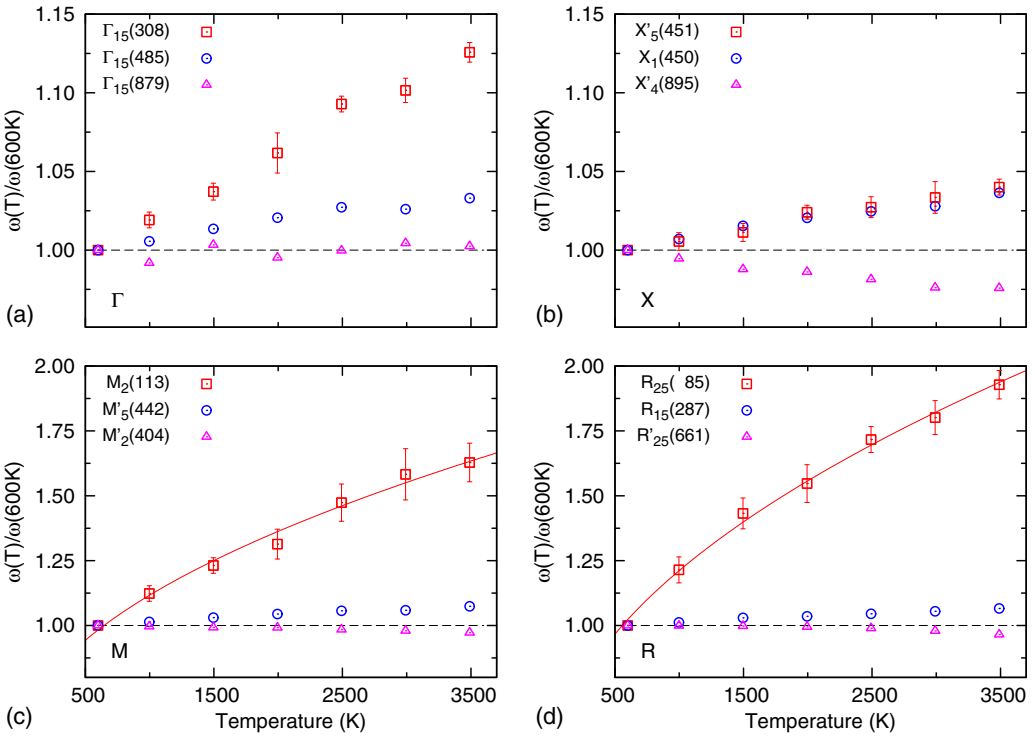


FIG. 6. (Color online) Temperature dependence of renormalized phonon frequencies at constant volume. For each inequivalent **q** vector, Two modes with the largest positive and one mode with the largest negative temperature dependence are shown. Each mode is labeled by its symmetry and frequency at 600 K (shown in parentheses in units of $cm^{-1}$). The plotted frequency and error bar correspond to the mean value and variance of the frequencies of all symmetrically equivalent modes. Solid lines show the $\sqrt{T}$ temperature dependence.

anharmonic part of the free energy $F_A(T)$ from

$$\frac{F_A(T)}{N-1} = -k_B T \int_0^T \frac{dT'}{T'}\left[\frac{E(T')-E_0}{(N-1)k_B T'} - 3\right], \qquad (9)$$

where $E(T')$ is the statistical average of the total energy for the MD simulation carried out at temperature $T'$, $E_0$ is the static energy of the relaxed structure $a^+b^-b^-$, and $N$ is the total number of particles in the MD supercell. We found that an exponential function $f(x) = a[\exp(-x/r) - 1]$, where $a$ and $r$ are fitting parameters, gives the best fit to $[(E(T') - E_0)/(N-1)k_B T' - 3]$. Integrating this fitted function we get $F_A(T)$. The anharmonic part of the entropy $S_A$ was calculated from $S_A = -\partial F_A/\partial T$. To compare with PGM results, a constant offset was applied such that $S_A$ at 600 K was set to zero.

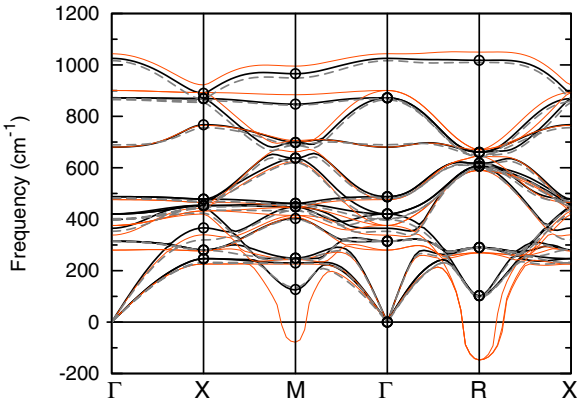


FIG. 7. (Color online) Phonon dispersions at 1000 K. The circles represent the frequencies extracted from the normal-mode correlation functions. Fourier interpolating these frequencies yields the renormalized phonon dispersions, shown in solid black line. Dashed lines are the phonon dispersions determined by fitting an effective harmonic force constant matrix [28]. Harmonic phonon dispersions calculated with DFPT are shown in orange (light) line.

Figure 8(a) shows the vibrational entropy $S_{vib}\{\tilde{\omega}(T)\}$ and $S_{vib}\{\tilde{\omega}(600\,K)\}$. We see that their difference is small, with the anharmonic entropy $S_A$ consisting of about 3% of the total entropy. This is because while some modes in cubic CaPv are strongly anharmonic, as shown in Fig. 6, the proportion of such modes is small. The harmonic part of the entropy still dominates. Accordingly, the thermal equations of states of cubic CaPv based on harmonic modes work fairly well [7,44,49,50]. On the other hand, a 3% difference in entropy is quite significant for determining properties such as phase boundaries [51,52]. In these cases, anharmonic effects need to be calculated accurately.

Figure 8(b) compares the anharmonic entropy calculated by TI and the one from PGM using Eq. (8). The agreement is quite good and consistent with similar tests on other systems [26]. While TI and PGM give very similar results when applied to the same supercell, the real advantage of PGM is that it can use phonon frequencies Fourier interpolated on a much denser **q** mesh, therefore overcoming the finite-size effect inherent in the TI approach. This feature is particularly important for AIMD, where the size of a simulation cell is seriously constrained by the current computational capacity [28].

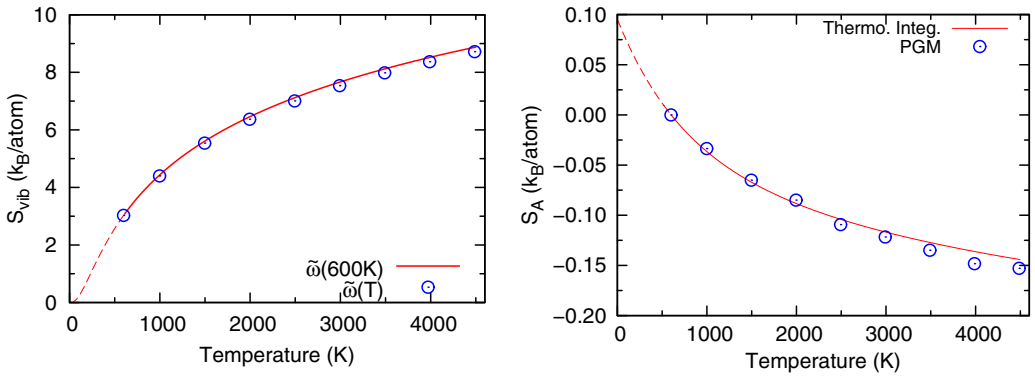


FIG. 8. (Color online) (a) Vibrational entropy predicted by PGM in the $2 \times 2 \times 2$ supercell. The line labeled as "$\tilde{\omega}$(600 K)" denotes the entropy calculated with phonon frequencies obtained at 600 K. Open circles with label "$\tilde{\omega}(T)$" are the entropies calculated with phonon frequencies at the corresponding temperatures. (b) Anharmonic entropy of cubic CaPv determined by TI (line) vs the one from PGM using Eq. (8) (circles) in the $2 \times 2 \times 2$ supercell. The system at 600 K is chosen as the reference state.

## VI. CONCLUSIONS

We have used a recently proposed hybrid scheme [23] that combines *ab initio* molecular dynamics and lattice dynamics to study the dynamic stabilization of cubic CaPv at high-temperature and high-pressure conditions. In contrast with the other system previously investigated with this method, $MgSiO_3$ perovskite [23], CaPv is strongly anharmonic. Here, we presented the first test of this approach to a strongly anharmonic system. We witness the emergence of the cubic phase of CaPv from both the real space perspective (in terms of atomic vibrations) and the phase space perspective (in terms of phonons). The transition takes place at $T \sim 600$ K and $\sim$26 GPa, in agreement with some experiments. In particular, we show that phonon quasiparticles are well defined once the cubic phase is stabilized. With this knowledge, we are able to characterize systematically intrinsic anharmonic frequency shifts in cubic CaPv. In contrast with direct free-energy methods such as thermodynamic integration, the current methodology offers a realistic approach for *ab initio* free-energy calculations in the thermodynamic limit ($N \to \infty$). Altogether, the current results validate the proposed methodology and invite further investigation of CaPv over temperature and pressure ranges of geophysical significance.

## ACKNOWLEDGMENTS

We thank P. B. Allen and K. Umemoto for useful discussions. We also thank K. Umemoto for supplying us with the pseudopotentials used in this work. This work was primarily supported by NSF Grants No. EAR-1047626 and No. EAR-0810272. D-BZ was supported primarily by the Abu Dhabi-Minnesota Institute for Research Excellence; a partnership between the Petroleum Institute of Abu Dhabi and the Department of Chemical Engineering and Materials Science of the University of Minnesota. Computational resources were provided by the Minnesota Supercomputing Institute and Extreme Science and Engineering Discovery Environment (https://www.xsede.org).

[1] L. Stixrude, R. Cohen, R. Yu, and H. Krakauer, Am. Mineral. **81**, 1293 (1996).
[2] S. Shim, R. Jeanloz, and T. Duffy, Geophys. Res. Lett. **29**, 2166 (2002).
[3] R. M. Wentzcovitch, Y. G. Yu, and Z. Wu, Rev. Mineral. Geochem. **71**, 59 (2010).
[4] R. M. Wentzcovitch, Z. Wu, and P. Carrier, Rev. Mineral. Geochem. **71**, 99 (2010).
[5] L. G. Liu and A. E. Ringwood, Earth Planet. Sci. Lett. **28**, 209 (1975).
[6] Y. Wang and D. J. Weidner, Geophys. Res. Lett. **21**, 895 (1994).
[7] Y. Wang, D. J. Weidner, and F. Guyot, J. Geophys. Res. **101**, 661 (1996).
[8] R. M. Wentzcovitch, N. L. Ross, and G. D. Price, Phys. Earth Planet. Int. **90**, 101 (1995).
[9] T. Kurashina, K. Hirose, S. Ono, N. Sata, and Y. Ohishi, Phys. Earth Planet. Int. **145**, 67 (2004).
[10] S. Ono, Y. Ohishi, and K. Mibe, Am. Mineral. **89**, 1480 (2004).
[11] L. Stixrude, C. Lithgow-Bertelloni, B. Kiefer, and P. Fumagalli, Phys. Rev. B **75**, 024108 (2007).
[12] R. Caracas, R. Wentzcovitch, G. D. Price, and J. Brodholt, Geophys. Res. Lett. **32**, L06306 (2005).
[13] R. Caracas and R. M. Wentzcovitch, Acta Crystallogr. B **62**, 1025 (2006).
[14] D. Y. Jung and A. R. Oganov, Phys. Chem. Miner. **32**, 146 (2005).
[15] D. J. Adams and A. R. Oganov, Phys. Rev. B **73**, 184106 (2006).
[16] T. Komabayashi, K. Hirose, N. Sata, Y. Ohishi, and L. S. Dubrovinsky, Earth Planet. Sci. Lett. **260**, 564 (2007).
[17] T. Uchida, Y. Wang, N. Nishiyama, K.-i. Funakoshi, H. Kaneko, A. Nozawa, R. B. Von Dreele, M. L. Rivers, S. R. Sutton, A. Yamada, T. Kunimoto, T. Irifune, T. Inoue, and B. Li, Earth Planet. Sci. Lett. **282**, 268 (2009).
[18] Y. Kudo, K. Hirose, M. Murakami, Y. Asahara, H. Ozawa, Y. Ohishi, and N. Hirao, Earth Planet. Sci. Lett. **349**, 1 (2012).

[19] L. Li, D. J. Weidner, J. Brodholt, D. Alfè, G. David Price, R. Caracas, and R. Wentzcovitch, Phys. Earth Planet. Int. **155**, 249 (2006).
[20] L. Li, D. J. Weidner, J. Brodholt, D. Alfè, G. D. Price, R. Caracas, and R. Wentzcovitch, Phys. Earth Planet. Int. **155**, 260 (2006).
[21] M. T. Dove, *Introduction to Lattice Dynamics* (Cambridge University, Cambridge, 1993).
[22] M. Dove, Am. Mineral. **82**, 213 (1997).
[23] D.-B. Zhang, T. Sun, and R. M. Wentzcovitch, Phys. Rev. Lett. **112**, 058501 (2014).
[24] D. C. Wallace, *Thermodynamics of Crystals* (Wiley, New York, 1972).
[25] G. Grimvall, *Thermophysical Properties of Materials*, revised ed. (North Holland, Amsterdam, 1999).
[26] T. Sun and P. B. Allen, Phys. Rev. B **82**, 224305 (2010).
[27] P. Souvatzis, O. Eriksson, M. I. Katsnelson, and S. P. Rudin, Phys. Rev. Lett. **100**, 095901 (2008).
[28] O. Hellman, I. A. Abrikosov, and S. I. Simak, Phys. Rev. B **84**, 180301(R) (2011).
[29] C. Lee, D. Vanderbilt, K. Laasonen, R. Car, and M. Parrinello, Phys. Rev. B **47**, 4863 (1993).
[30] C. Z. Wang, C. T. Chan, and K. M. Ho, Phys. Rev. B **42**, 11276 (1990).
[31] X. Gonze, J.-C. Charlier, D. C. Allan, and M. P. Teter, Phys. Rev. B **50**, 13035(R) (1994).
[32] G. D. Mahan, *Many-Particle Physics*, 2nd ed. (Plenum, New York, 1990).
[33] P. Giannozzi, S. Baroni, N. Bonini, M. Calandra, R. Car, C. Cavazzoni, D. Ceresoli, G. L. Chiarotti, M. Cococcioni, I. Dabo, A. Dal Corso, S. de Gironcoli, S. Fabris, G. Fratesi, R. Gebauer, U. Gerstmann, C. Gougoussis, A. Kokalj, M. Lazzeri, L. Martin-Samos, N. Marzari, F. Mauri, R. Mazzarello, S. Paolini, A. Pasquarello, L. Paulatto, C. Sbraccia, S. Scandolo, G. Sclauzero, A. P. Seitsonen, A. Smogunov, P. Umari, and R. M. Wentzcovitch, J. Phys.: Condens. Matter **21**, 395502 (2009).
[34] S. Baroni, S. de Gironcoli, A. Dal Corso, and P. Giannozzi, Rev. Mod. Phys. **73**, 515 (2001).
[35] J. P. Perdew and A. Zunger, Phys. Rev. B **23**, 5048 (1981).
[36] D. Vanderbilt, Phys. Rev. B **41**, 7892 (1990).
[37] R. A. Cowley, Rep. Prog. Phys. **31**, 123 (1968).
[38] H. J. Monkhorst and J. D. Pack, Phys. Rev. B **13**, 5188 (1976).
[39] R. M. Wentzcovitch and J. L. Martins, Sol. Stat. Comm. **78**, 831 (1991).
[40] W. G. Hoover, Phys. Rev. A **31**, 1695 (1985).
[41] W. H. Press, B. P. Flannery, S. A. Teukolsky, and W. T. Vetterling, *Numerical Recipes in Fortran 77*, 1st ed., Numerical Recipes: The Art of Scientific Computing Vol. 1 (Cambridge University, Cambridge, 1986).
[42] A. Glazer, Acta Crystallogr. B **28**, 3384 (1972).
[43] G. J. Martyna, M. L. Klein, and M. Tuckerman, J. Chem. Phys. **97**, 2635 (1992).
[44] M. Noguchi, T. Komabayashi, K. Hirose, and Y. Ohishi, Phys. Chem. Miner. **40**, 81 (2012).
[45] N. de Koker, Phys. Rev. Lett. **103**, 125902 (2009).
[46] R. A. Cowley, Phys. Rev. **134**, A981 (1964).
[47] L. L. Boyer and J. R. Hardy, Phys. Rev. B **24**, 2577 (1981).
[48] M. P. Allen and D. J. Tildesley, *Computer Simulation of Liquids* (Clarendon, Oxford, 1987).
[49] Y. Zhang, D. Zhao, M. Matsui, and G. Guo, Phys. Chem. Miner. **33**, 126 (2006).
[50] Z. J. Liu, X. W. Sun, Q. F. Chen, L. C. Cai, H. Y. Wu, and S. H. Ge, J. Phys.: Condens. Matter **19**, 246103 (2007).
[51] Z. Wu and R. M. Wentzcovitch, Phys. Rev. B **79**, 104304 (2009).
[52] B. Fultz, Prog. Mater. Sci. **55**, 247 (2010).